Journal of Zhejiang University-SCIENCE C (Computers & Electronics)
ISSN 1869-1951 (Print); ISSN 1869-196X (Online)
www.zju.edu.cn/jzus; www.springerlink.com
E-mail: jzus@zju.edu.cn

Automatic mass segmentation on mammograms combining random walks and active contour*

Xin HAO[†1], Ye SHEN[1,2], Shun-ren XIA[†‡1]

([1]*MOE Key Laboratory of Biomedical Engineering, Zhejiang University, Hangzhou 310027, China*)

([2]*Department of Signal and Information Processing, China Jiliang University, Hangzhou 310018, China*)

[†]E-mail: sarah.xin@gmail.com; srxia@zju.edu.cn

Received Mar. 6, 2012; Revision accepted July 12, 2012; Crosschecked Aug. 3, 2012

Abstract: Accurate mass segmentation on mammograms is a critical step in computer-aided diagnosis (CAD) systems. It is also a challenging task since some of the mass lesions are embedded in normal tissues and possess poor contrast or ambiguous margins. Besides, the shapes and densities of masses in mammograms are various. In this paper, a hybrid method combining a random walks algorithm and Chan-Vese (CV) active contour is proposed for automatic mass segmentation on mammograms. The data set used in this study consists of 1095 mass regions of interest (ROIs). First, the original ROI is preprocessed to suppress noise and surrounding tissues. Based on the preprocessed ROI, a set of seed points is generated for initial random walks segmentation. Afterward, an initial contour of mass and two probability matrices are produced by the initial random walks segmentation. These two probability matrices are used to modify the energy function of the CV model for prevention of contour leaking. Lastly, the final segmentation result is derived by the modified CV model, during which the probability matrices are updated by inserting several rounds of random walks. The proposed method is tested and compared with other four methods. The segmentation results are evaluated based on four evaluation metrics. Experimental results indicate that the proposed method produces more accurate mass segmentation results than the other four methods.

Key words: Active contour, Random walks, Mass segmentation, Mammogram
doi:10.1631/jzus.C1200052 **Document code:** A **CLC number:** TP391.41

1 Introduction

Breast cancer is a leading cause of cancer death in women in many countries (Hong and Sohn, 2010). Numerous studies have shown that early detection saves lives and increases treatment options. The earlier sign of breast cancer is often detected on a mammogram, before it can be felt by the woman or a health care professional (American Cancer Society, 2011). The computer-aided diagnosis (CAD) system for mammography aims to detect and characterize the suspicious regions in order to provide a second opinion of breast cancer diagnosis.

Mass is one of the major abnormities in mammogram. The mammographic mass analysis is based on the mass shape, margin, and density (Ball and Bruce, 2007b). Therefore, mass segmentation is a critical step in mammogram CAD systems. The segmented contour of mass should be close to the actual boundary to provide feasible features for subsequent diagnostic decision support. Masses in mammograms possess various scales, complex shapes, and ambiguous margins. Some of them are embedded and hidden in surrounding parenchymal tissues (Wang *et al.*, 2011). Thus, mass segmentation is a challenging task. In recent years, there have been numerous studies on mass segmentation.

The region-growing algorithm is a typical image segmentation approach. Many extensions of region growing have been proposed to adapt to the mass segmentation problem (Guliato *et al.*, 1998; 2003;

‡ Corresponding author

* Project (Nos. 60772092 and 81101903) supported by the National Natural Science Foundation of China

Kupinski and Giger, 1998; Petrick *et al.*, 1999; Xu *et al.*, 2006; Cao *et al.*, 2009). The gradient information of boundary was also widely used in earlier mass segmentation methods. te Brake and Karssemeijer (2001) segmented masses with discrete dynamic contour, in which the external energy was determined by image gradient magnitude. Subsequently, different information was incorporated in mass segmentation methods. Timp and Karssemeijer (2004) first applied the dynamic programming boundary tracing (DPBT) technique to mass segmentation. The heart of DPBT is the local cost function, which is formed by edge strength, mass size, and intensity. This method was improved by several studies (Domínguez and Nandi, 2007; Hao and Xia, 2009; Song *et al.*, 2009; 2010). The active contour model was also commonly used in mass segmentation, since it is flexible and effective in capturing complex topologies (Sahiner *et al.*, 2001; Xiao *et al.*, 2005; Ball and Bruce, 2007a; Yuan *et al.*, 2007; Wang *et al.*, 2011).

In general, most of these traditional methods focus on the establishment of appropriate object models and developing algorithms to find the parameters for these models (Grady, 2006). The adaptability of these methods is limited due to the complexity of masses. Earlier segmentation methods using the region-growing algorithm or gradient information easily fail due to the ambiguous margins of some masses. Although some methods, such as the CV model, can segment objects whose boundaries are not defined by gradients (Chan and Vese, 2001), they still cannot perform very well because some dense tissues surrounding masses present similar characteristics with masses. These surrounding dense tissues result in serious contour leaking problems. In addition, some masses possess highlights in the focal region with dimmer peripheral characteristics. This phenomenon induces the segmented contour to approach more to the inner region of mass, especially for malignant cases.

Grady (2006) proposed a supervised image segmentation algorithm based on random walks. Unlike traditional automatic approaches, the segmentation result was derived based on a set of pre-labeled pixels (seeds). There are three pragmatic properties of a random walks algorithm—weak boundary detection, noise robustness, and the assignment of ambiguous regions (Grady, 2006), which are beneficial to the mass segmentation problem. But the manual labeling of seed points is time consuming and is easily affected by many factors. Therefore, the traditional random walks algorithm can only be regarded as a semi-automatic method. In our previous work (Cao *et al.*, 2011), a region-growing algorithm was introduced to generate the seeds automatically. But the poor performance of region growing on masses with ambiguous margins and surrounding tissues degraded the performance of random walks.

In this study, we present a hybrid method combining a random walks algorithm and CV active contour for automatic mass segmentation. This method first preprocesses the original ROI to suppress noise and surrounding tissues. Based on the preprocessed ROI, a set of seeds for initial random walks segmentation is extracted from the isocontour map. Then, an initial contour of mass and two probability matrices are produced by the initial random walks segmentation. These two probability matrices are used to modify the energy function of the CV model. The final segmentation result is derived by the modified CV model. During the contour evolution, the probability matrices are updated by inserting several rounds of random walks. The proposed method has the following properties:

1. After the preprocessing step, the isocontour map shows steady performance on the automatic acquisition of seeds. The background seeds are defined as a shape constraint to prevent contour leaking.

2. The energy function of the CV model is modified by the probability matrices produced by random walks. This modification can prevent the contour leaking problem due to the shape constraint effect and weak boundary detection property of random walks.

3. The final result is derived by the modified CV model, which is more effective in capturing complex shapes of masses.

4. The update of probability matrices during contour evolution avoids the segmented region from shrinking to the focal region of mass. Thus, some ambiguous characteristics in the periphery of mass can be captured.

2 Previous work and the data set

2.1 Chan-Vese model

Chan and Vese (2001) proposed an active contour model without edges to detect object in an image.

The Chan-Vese model can segment objects whose boundaries are not defined by gradients. The energy function was established based on the assumption that the image u_0 was formed by two regions with approximately piecewise constant intensities of distinct values. Denoting its boundary by C, the energy function $F(c_1, c_2, C)$ is defined as

$$\begin{aligned} F(c_1,c_2,C) &= \mu\cdot\text{Length}(C) \\ &+\lambda_1\int_{\text{inside}(C)}|u_0(x,y)-c_1|^2\,\text{d}x\text{d}y \\ &+\lambda_2\int_{\text{outside}(C)}|u_0(x,y)-c_2|^2\,\text{d}x\text{d}y, \end{aligned} \tag{1}$$

where $\mu\geq 0$, λ_1, $\lambda_2>0$ are fixed parameters, and c_1, c_2 are mean values inside and outside the evolving contour C, respectively. The first term in Eq. (1) is the regularization term which prevents the final contour from converging to a small area due to noise (Yuan *et al.*, 2007). The last two terms are fitting terms.

2.2 Random walks for image segmentation

The random walks algorithm (Grady, 2006) is a supervised graph-based approach for image segmentation. In the case of mass segmentation, two kinds of pre-labeled seeds indicating regions of the image belonging to mass or background are first provided. Then, the algorithm determines the label of an unseeded pixel by resolving the following problem: Given a random walker starting at this location, what is the probability that it first reaches a mass seed before it reaches a background seed? If the probability is above 0.5, this pixel is assigned as mass. Otherwise, it is assigned as background.

It has been previously established that the probability that a random walker first reaches a seed point exactly equals the solution to the Dirichlet problem with boundary conditions at the locations of the seeds. To solve this problem, the image is treated as a graph with a fixed number of vertices and edges. As described in Grady (2006), the typical Gaussian weighting function is chosen to map the changes of image intensities to edge weights as

$$w_{ij}=\exp[-\beta(g_i-g_j)^2], \tag{2}$$

where g_i indicates the image intensity at pixel i, and β represents the only free parameter in the random walks algorithm.

For mass segmentation, two kinds of seeds indicating mass and background should be generated automatically. Each segmented region generated by random walks is guaranteed to be connected to seeds with the same label. There is no isolated region of a particular label that contains no seeds (Grady, 2006). Therefore, the mass seeds should be labeled inside the mass region. Meanwhile, if we set the background seeds as an enclosed contour surrounding the mass, the segmented region will never cross the contour of background seeds. Hence, the background seeds can be considered as the shape constraint for preventing contour leaking. In this paper, we introduce the intensity based topographic representation of an image called the isocontour map to derive the seed points.

2.3 Isocontour map

Consider image $I:\Omega\subset\mathbb{R}^2\rightarrow\mathbb{R}^+$ to be a surface elevation $\phi\subset\mathbb{R}^3$ in intensity:

$$\phi:\boldsymbol{x}\rightarrow I(\boldsymbol{x}),\ \ \boldsymbol{x}\in\Omega, \tag{3}$$

where Ω is the domain of image $I(\boldsymbol{x})$. Then, the isocontours $\Gamma(t)$ of a given intensity level $t\in\mathbb{R}^+$ are defined as the boundaries of the compact and connected regions $R(t)\subset\Omega$, where the pixel intensities are higher than t:

$$R(t)=\{\boldsymbol{x}\,|\,\phi(\boldsymbol{x})>t\},\ \Gamma(t)=\partial R(t). \tag{4}$$

Based on the definitions above, the isocontour map is generated from a set of isocontours at multiple distinct partition values over the intensity range of the image (Hong and Sohn, 2010):

$$\begin{cases} M_N(I)=\{\Gamma(t_i)\,|\,i=1,2,\cdots,N\}, \\ t_i=t_{\max}-(i-1)\Delta t, \\ \Delta t=(t_{\max}-t_{\min})/(N-1), \end{cases} \tag{5}$$

where $M_N(I)$ is the isocontour map of image I with N levels of quantizations, $t_{\min}$ and $t_{\max}$ are the minimum and maximum intensities of I respectively, and Δt is the interval of the partition intensities.

There are some salient features of an isocontour map of a mass in mammograms (Hong and Sohn,

2010). As shown in Fig. 1, the isocontours within a mass generally form a nested pattern, and the nested pattern is denser near the boundary of mass. In addition, the shapes of isocontours extending from interior to exterior of the mass gradually approach to that of the object boundary. Therefore, if we can extract the isocontour $\Gamma(t')$ of certain intensity level t', which is close to the actual mass boundary (Fig. 1c), it will be adaptive to define $\Gamma(t')$ as the background seeds of random walks. Then, it is also convenient to define an isocontour inside $\Gamma(t')$ as the mass seeds.

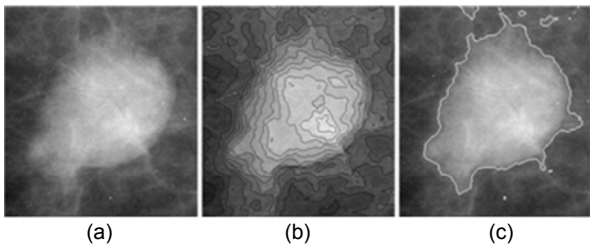

Fig. 1 An example of the isocontour map of mass region of interest (ROI)

(a) Original mass ROI; (b) Isocontour map of (a); (c) Isocontour on a certain intensity level

The extraction of the isocontour can be affected by noise and surrounding tissues (Hong and Sohn, 2010). Thus, the original ROIs are preprocessed to smooth the image and suppress surrounding tissues.

2.4 Data set

All the mammograms used in this study are from the Digital Database for Screening Mammography (DDSM) at the University of South Florida (Heath *et al.*, 1998; 2000). In this study, 1066 mammograms with masses are collected from 674 cases. The resolution of mammograms is scaled down to 100 micron per pixel, and the range of gray level is reduced from 12/16 bits to 8 bits.

A set of 1095 mass ROIs (570 benign, 525 malignant) is first extracted from the mammograms according to the rough outlines of lesions provided by DDSM. Then, a manual segmentation of each ROI is produced by experienced radiologists. These manually segmented regions are treated as ground truth in our experiments. The geometric center of each mass is generated according to the manual segmentation. In the practical mammogram CAD system, the geometric center can be provided by the previous lesion detection.

The data set includes masses with different shapes, margin types (Fig. 2) and different sizes (Table 1), from mammograms with different breast tissue densities (Table 1). The size of mass is measured by the effective radius of area inside the contour delineated by radiologists (Song *et al.*, 2010).

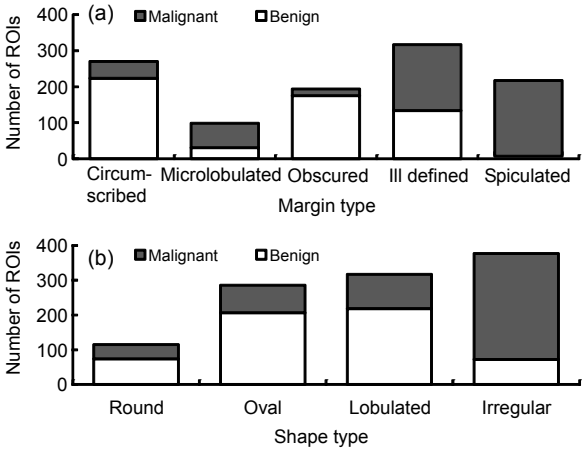

Fig. 2 Distribution of different margin (a) and shape (b) types of masses

Table 1 Distribution of masses with different sizes and breast tissue densities

Statistic	Mass size (mm)	Breast tissue density	Number of masses
Minimum	2.5	1: Entirely fatty	272
0.25 Quartile	5.2	2: Scattered fibroglandular	520
Median	7.0	3: Heterogenously dense	227
Mean	8.0	4: Extremely dense	76
0.75 Quartile	9.2		
Maximum	31.2		

3 Segmentation of mass

The proposed method consists of three stages (Fig. 3). First, the original ROI is preprocessed to suppress noise and surrounding tissues. Then, the random walks algorithm is employed to obtain the initial boundary of mass and generate two probability matrices. Finally, the CV model is modified to obtain the segmentation result. Note that the preprocessed ROI is used only to generate the seeds for initial random walks. The segmentation processes in second and third stages are performed on the original ROI.

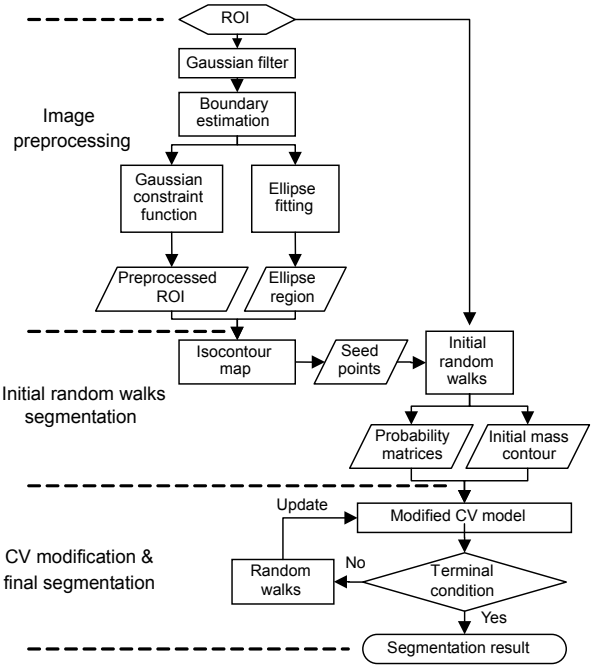

Fig. 3 Flow chart of the proposed segmentation method consisting of three stages

3.1 Image preprocessing

To obtain a continuous curve for the isocontour, it is necessary to smooth the ROI. In this study, the original mass ROI $I(x, y)$ is first smoothed by a Gaussian filter G_{smooth} with predefined standard deviation σ_s=1.5. Then, the filtered ROI is multiplied with an isotropic Gaussian constraint function (Kupinski and Giger, 1998) $G_{\text{constraint}}(x, y, \sigma_c^2)$ centered at the geometric center of mass. Due to the intensity distribution of $G_{\text{constraint}}$ (Fig. 4c), it can suppress the surrounding tissues (Fig. 4d) and strengthen the nested pattern of the isocontour map (Fig. 4f).

To set the size parameter σ_c of $G_{\text{constraint}}$ adaptively, we implement a mass boundary estimation process (Domínguez and Nandi, 2007) before generating the corresponding $G_{\text{constraint}}$. A set of discrete boundary pixels of mass is generated by measuring the differences between mean values at different locations moving from interior to exterior of the mass (for details, see Domínguez and Nandi (2007)). Then, the size σ_c is set as 1.5 times the average location of the estimated boundary pixels. Moreover, we fit these estimated pixels into an ellipse by least squares methods (Fig. 4e). It can be seen that the fitted ellipse roughly covers the mass region.

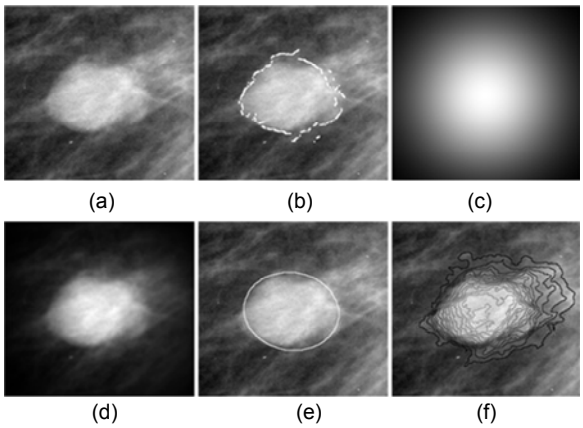

Fig. 4 An example of ROI preprocessing
(a) Original mass ROI; (b) Estimated boundary pixels of mass in (a); (c) Gaussian constraint function; (d) Preprocessed ROI multiplied with the Gaussian constraint function; (e) Fitted ellipse according to (b); (f) Isocontour map of preprocessed ROI at 14 intensity levels

3.2 Initial random walks segmentation

To label the seeds of the initial random walks automatically, we generate the isocontour map of the preprocessed ROI $I'(x, y)$ as

$$\begin{cases} M_N(I') = \{\Gamma(t_i) \mid i = 1, 2, \cdots, N\}, \\ t_i = t_{\max} - (i-1)\Delta t, \end{cases} \tag{6}$$

where $\Gamma(t_i)$ are the isocontours of intensity level t_i, $t_{\max}$ is the maximum intensity of $I'(x, y)$, and N denotes the number of intensity levels. The intensity interval Δt is set as 10 in this study. At each intensity level, only the isocontour surrounding the mass center is reserved, since the background seeds should be defined as an enclosed contour surrounding the mass. The isocontour map of a preprocessed ROI at 14 intensity levels is shown in Fig. 4f. It is clear that isocontour $\Gamma(t_i)$ extends from interior to exterior of mass with the decrease of intensity level t_i.

According to the properties of the isocontour map analyzed in Section 2.3, we want to extract an isocontour that is close to the actual mass boundary. This isocontour will be set as the background seed in order to constrain the segmented region from contour leaking. For this purpose, the initial ellipse region obtained in the preprocessing stage (Section 3.1) will be used.

Let $A(t_i)$ be the area of region $R(t_i)$ inside an isocontour $\Gamma(t_i)$, and A_{ellipse} be the area of the ellipse region. Since the ellipse roughly covers the mass, region $R(t_i)$ with area $A(t_i)$ close to A_{ellipse} will also cover the mass region. In addition, because the isocontours extending from interior to exterior of mass gradually approach to the mass boundary, the corresponding isocontour $\Gamma(t_i)$ will be close to the mass boundary.

According to above discussions, we summarize the acquisition of seeds as follows:

Step 1: Set intensity level as $t_i=t_{\max}$ and initialize the iteration number as $i=0$.

Step 2: Obtain the isocontour $\Gamma(t_i)$ that surrounds the mass center.

Step 3: Compare the current $A(t_i)$ with A_{ellipse}.

If $A(t_i)<A_{\text{ellipse}}$, add 1 to the iteration number i. Then, update the intensity level as $t_i=t_{i-1}-\Delta t$ and repeat Step 2 and Step 3.

If $A(t_i)\geq A_{\text{ellipse}}$, go to Step 4.

Step 4: Dilate the current region $R(t_i)$ by a disk-shaped structure element. The radius of this element is set as 10 pixels by experiments to ensure that the dilated region can cover the mass. Then, the boundary of the dilated region is defined as background seeds.

Step 5: The isocontour inside background seeds with area near $A_{\text{ellipse}}/2$ is defined as mass seeds. The ratio of 1/2 is selected in experiments to ensure that mass seeds are labeled inside the mass region.

Based on these seeds (Fig. 5a), the initial random walks segmentation is implemented. As described in Section 2.2, each unlabeled pixel (x, y) will be assigned a probability $P_{\text{m}}(x, y)$ that the random walker starting at (x, y) reaches a mass seed before it reaches a background seed. Since there are only two kinds of seeds, the probability that the random walker reaches a background seed before a mass seed is solved by

$$P_{\text{b}}(x,y)=1-P_{\text{m}}(x,y),\quad 0\leq P_{\text{b}},P_{\text{m}}\leq 1. \tag{7}$$

Pixels with P_{m} above 0.5 are labeled as mass. Otherwise, they are labeled as background. The initial contour and the probability matrices of $\boldsymbol{P}_{\text{m}}$ and $\boldsymbol{P}_{\text{b}}$ are illustrated in Figs. 5b–5d. The P_{m} values of pixels outside the background seeds are assigned as zero, which demonstrates the effect of the shape constraint.

By the initial random walks segmentation the rough regions of masses can be found. However, the initial contours approach more to the inner regions of masses, especially for malignant cases. This phenomenon results from the intensity distribution of masses. Masses in mammograms possess highlight focal regions with dimmer and subtle structures in the periphery. These peripheral structures are easily suppressed in the preprocessing step. It is also difficult to label appropriate seeds for these peripheral structures even without preprocessing. To address this problem, a modified active contour model is proposed to refine the segmentation results.

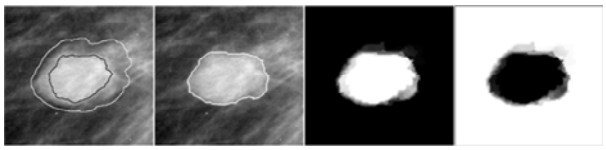

Fig. 5 An example of initial random walks segmentation
(a) Background seeds (white contour) and mass seeds (black contour) of Fig. 4a; (b) Initial mass contour of Fig. 4a; (c) Probability matrix of $\boldsymbol{P}_{\text{m}}$; (d) Probability matrix of $\boldsymbol{P}_{\text{b}}$

3.3 CV model modification and mass segmentation

The contour evolution of the conventional CV model is forced mainly by minimizing the fitting terms of the energy function (Chan and Vese, 2001):

$$\begin{aligned}F_1(C)+F_2(C)=&\lambda_1\int_{\text{inside}(C)}\left|I(x,y)-c_1\right|^2\mathrm{d}x\mathrm{d}y\\&+\lambda_2\int_{\text{outside}(C)}\left|I(x,y)-c_2\right|^2\mathrm{d}x\mathrm{d}y.\end{aligned} \tag{8}$$

But the fitting terms consider only the intensity distribution of foreground and background. Therefore, serious contour leaking will occur if the surrounding tissues possess similar intensities as the masses.

Unlike the conventional CV model, the random walks algorithm generates the segmentation results based on some predefined seeds, which can effectively constrain the segmentation results. Thus, if we can combine these two algorithms properly, more accurate mass boundaries should be captured. In this study, two probability matrices $\boldsymbol{P}_{\text{m}}$ and $\boldsymbol{P}_{\text{b}}$ produced by the initial random walks are used to modify the fitting terms:

$$\begin{aligned}&F_1(C)+F_2(C)\\&=\lambda_1\int_{\text{inside}(C)}P_{\text{b}}(x,y)\left|I(x,y)-c_1\right|^2\mathrm{d}x\mathrm{d}y\\&\quad+\lambda_2\int_{\text{outside}(C)}P_{\text{m}}(x,y)\left|I(x,y)-c_2\right|^2\mathrm{d}x\mathrm{d}y.\end{aligned} \tag{9}$$

In the modified function, the energy of each pixel formulated as $|I(x, y)-c_1|^2$ or $|I(x, y)-c_2|^2$ is weighted by the corresponding probability $P_b(x, y)$ or $P_m(x, y)$. Therefore, the energy of each pixel is not only determined by its intensity, but also modulated by the probability of random walks. For instance, if the region inside contour C covers some pixels of surrounding tissues, whose P_b values are much higher, the energy of $F_1(C)$ will increase.

In the level set method (Osher and Sethian, 1988), contour C is represented implicitly by the zero level set of a 3D Lipschitz function ϕ. The corresponding level set formulation of the modified energy function is derived as

$$\begin{aligned}\frac{\partial\varphi}{\partial t} &= \delta_\varepsilon[\mu\cdot\mathrm{div}(\nabla\varphi/\|\nabla\varphi\|)\\ &\quad -\lambda_1 P_b(I-c_1)^2+\lambda_2 P_m(I-c_2)^2],\end{aligned} \tag{10}$$

where δ_ε is a slightly regularized 1D Dirac measure δ_0 (Chan and Vese, 2001). The initial contour of the evolution is set as the result of initial random walks (Section 3.2) and refined by the modified CV model.

As discussed in Section 3.2, the segmented contour of initial random walks approaches more to the inner region of mass. This phenomenon indicates that the probability matrices produced by initial random walks are not appropriate enough. Therefore, if the CV model is modified only by the initial probability matrices, the contour evolution will also shrink to the inner region of mass (Fig. 6a).

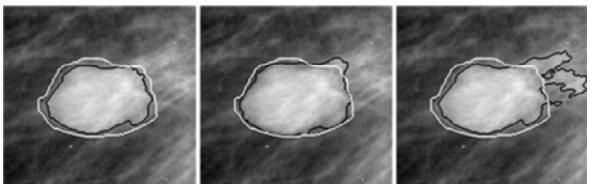

Fig. 6 Manual segmentation (white contour) and automatic segmentation (black contour) of modified CV without probability update (a), modified CV with probability update (b), and the conventional CV model (c)

To address this problem, we execute several rounds of random walks during the contour evolution process in order to update the probability matrices. The inserted random walks process aims to explore the peripheral region of the current contour in order to capture the subtle or ambiguous margin information of mass. For this purpose, we define the seeds of the inserted random walks as follows:

Let C be the current contour after several rounds of evolution, and R be the region inside C.

Step 1: Define mass seeds as current contour C.

Step 2: Dilate region R by a disk-shaped structure element with a radius of 10 pixels.

Step 3: Define the boundary of the dilated region as background seeds.

Thus, the inserted random walks can explore an annular region outside the current contour.

The inserted random walks process is executed after every n iterations of contour evolution. The execution frequency n is determined as 50 by experiments to balance the computation efficiency and segmentation accuracy. The convergence of the evolution is checked according to the change of length of contour (Chaudhury and Ramakrishnan, 2007). The maximum number of iterations N_{max} is also set as 250 in case the evolution cannot meet the convergence condition for some masses. Fig. 6b shows the segmented contour of the modified CV model with probability updates. It is closer to the actual mass boundary than Fig. 6a, and the contour leaking of the conventional CV model (Fig. 6c) is also prevented.

4 Experimental results

4.1 Evaluation metrics

The segmentation performance is assessed by comparing the computer delineated region with manual segmentation. The area overlap measure (AOM) is widely used to evaluate the segmentation performance:

$$\mathrm{AOM}=\frac{A_{seg}\cap A_{gs}}{A_{seg}\cup A_{gs}}, \tag{11}$$

where A_{seg} denotes the area of automatic segmentation and A_{gs} denotes the corresponding ground-truth area of manual segmentation

To evaluate the unsegmented mass (false negative) pixels and segmented nonmass (false positive) pixels, two metrics M_{FN} and M_{FP} (Qian *et al.*, 1999) are also considered in this study:

$$\begin{cases} M_{\mathrm{FN}} = [A_{\mathrm{gs}} - (A_{\mathrm{seg}} \cap A_{\mathrm{gs}})] / A_{\mathrm{gs}}, \\ M_{\mathrm{FP}} = [A_{\mathrm{seg}} - (A_{\mathrm{seg}} \cap A_{\mathrm{gs}})] / A_{\mathrm{seg}}. \end{cases} \tag{12}$$

In addition, the average minimum Euclidean distance (AMED) is calculated in our experiments. Let $A=\{a_1, a_2, \ldots, a_m\}$ and $B=\{b_1, b_2, \ldots, b_n\}$ denote two contours, and $d(a_i, B)$ denote the distance from a_i to the closest point on contour B. The AMED(A, B) is defined as

$$\mathrm{AMED}(A,B) = \max\left(\frac{1}{m}\sum_{i=1}^{m} d(a_i,B),\ \frac{1}{n}\sum_{j=1}^{n} d(b_j,A) \right), \tag{13}$$

where

$$d(a_i,B) = \min_{j\in\{1,2,\cdots,n\}} \left\| a_i - b_j \right\|.$$

4.2 Comparative experiments

In this subsection, we compare the segmentation performance of different methods as shown in Table 2. We slightly modify the original RGRW method (Cao *et al.*, 2011) by defining the background seeds in the same way as we have used in the initial random walks step (Section 3.2). This modification can effectively improve the performance of the original method.

The parameters of RGILS and TMDP methods are provided by Yuan *et al.* (2007) and Song *et al.* (2010), respectively. The parameters of RWCV, CVAC, and RGRW methods are selected by 5-fold cross-validation, respectively. The parameters of the random walks and CV active contour model used in our RWCV method are listed in Table 3.

Table 3 Parameters used in the proposed RWCV method

Parameter	Value	Equation
μ	0.05×255^2	Eq. (10)
λ_1, λ_2	1	Eq. (10)
β	90	Eq. (2)

Each ROI is segmented by all the five methods. The segmentation results are evaluated by four metrics of AOM, M_{FN}, M_{FP}, and AMED. Some descriptive statistics, such as the minimum, 0.25 quartile, mean, median, 0.75 quartile, and maximum values of these four metrics are calculated. Fig. 7

Table 2 Segmentation methods compared in our experiments

Reference	Description	Abbreviation
This paper	The proposed method combining random walks and the CV model	RWCV
Chan and Vese (2001)	The conventional CV model. The initial contour is set as the segmentation result of initial random walks (Section 3.2)	CVAC
Cao *et al.* (2011)	Our previous work on the random walks based method, in which the region growing is used to label the seeds automatically	RGRW
Yuan *et al.* (2007)	A dual-stage level set method, in which the radial gradient index (RGI) algorithm is applied to yield an initial contour	RGILS
Song *et al.* (2010)	A hybrid segmentation method using template matching and dynamic programming	TMDP

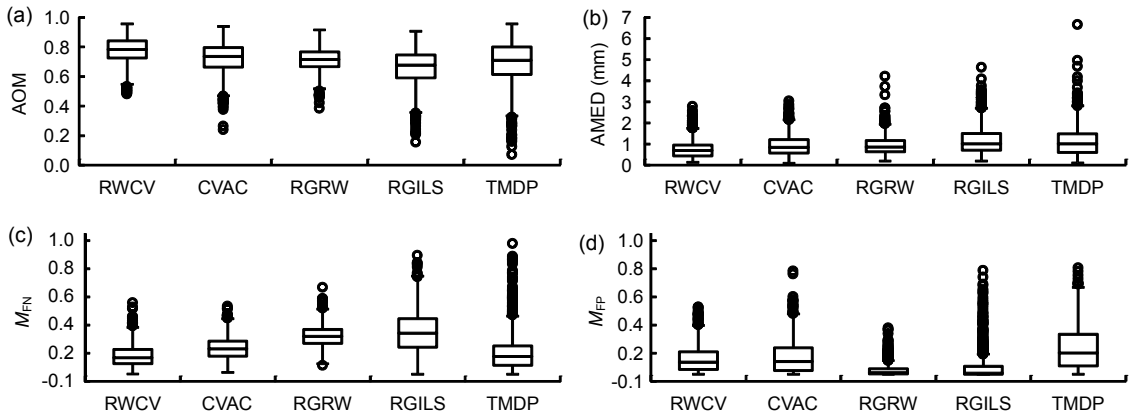

Fig. 7 Boxplots of the distribution of four evaluation metrics: (a) AOM; (b) AMED; (c) M_{FN}; (d) M_{FP}

shows the box and whisker plots of the distribution of the four evaluation metrics. The boxplots of AOM and AMED metrics (Figs. 7a and 7b) show that the proposed RWCV method has better performance than the other four methods. The differences between our RWCV method and the other four methods are statistically significant, since the P values of the Student's t test for the distribution of these four metrics of our method and the other four methods are all less than 0.001.

Fig. 8 shows several segmentation results using these five methods. It can be seen that the segmented contours of RGRW and RGILS methods are prone to shrink to the core regions of masses, and ignore some dimmer or subtle information in the periphery. This phenomenon is also supported by the M_{FN} and M_{FP} evaluations. As shown in Figs. 7c and 7d, the M_{FP} evaluations of RGRW and RGILS methods are better than those of the other three methods, but their M_{FN} evaluations are worse than those of the other methods. It means that the disagreements between the segmentation results of these two methods and manual segmentation come mainly from the false negative pixels. The CVAC method shows better performance on M_{FN} evaluation than the RGRW and RGILS methods. But it is also easier to be affected by the surrounding tissues. The TMDP method shows better performance on M_{FN} evaluation, but its M_{FP} is worse than those of the other four methods, indicating that poorer performance of TMDP mainly results from the false positive pixels. The results of our RWCV method are visually closer to the radiologist's outlines. The performance of the RWCV method on M_{FN} and M_{FP} metrics is better than those of other methods.

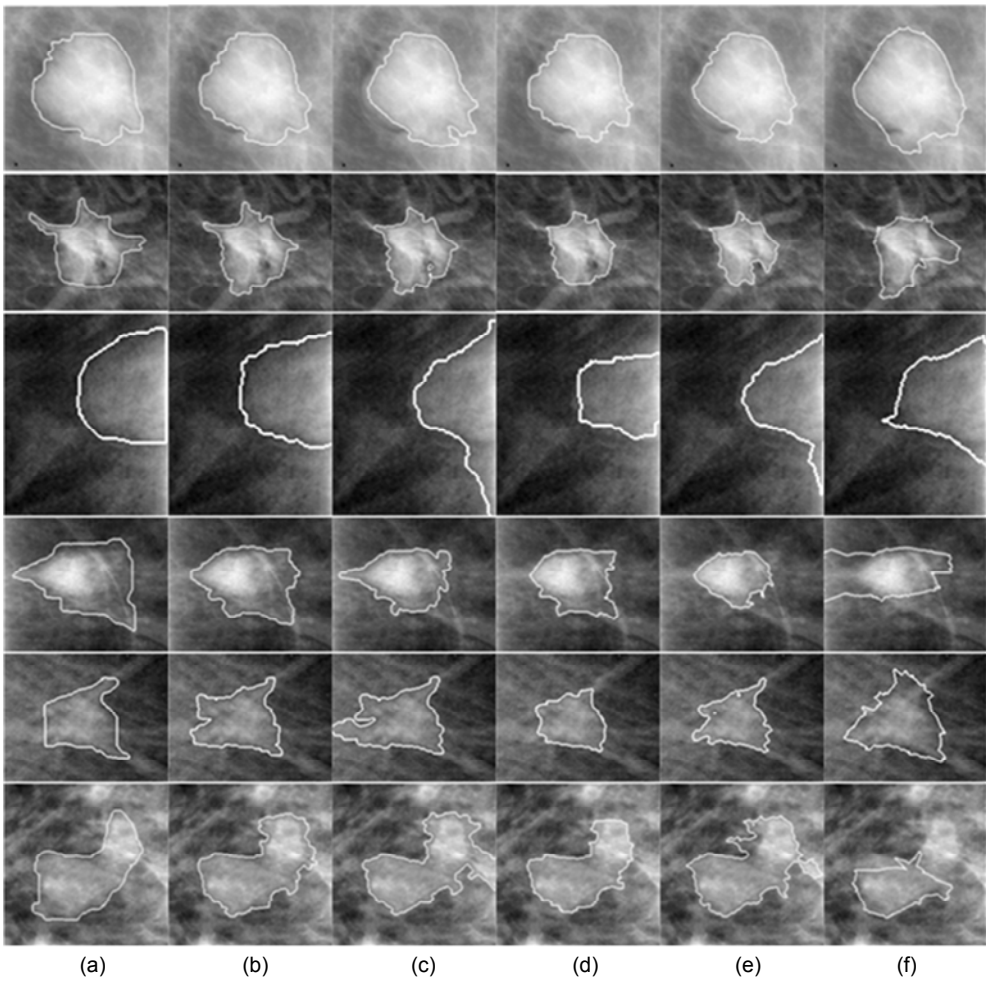

Fig. 8 Six instances of ground truth (a) and segmentation results of RWCV (b), CVAC (c), RGRW (d), RGILS (e), and TMDP (f)

Masses are benign in the first three rows, and malignant in the other three

As the shape and margin types of masses are important characteristics for the diagnosis of breast cancer, Figs. 9a and 9b show the segmentation performance of each method on different margin and shape types of masses, respectively. Our RWCV method outperforms the other four methods for all five margin types and four shape types. All five segmentation methods have worst performance on masses with spiculated margin or irregular shape.

Since it is difficult to identify and segment lesions on mammograms with dense breast tissues, the segmentation performance on different breast density levels is also tested (Fig. 9c). Our RWCV method shows better performance on all four levels. The performance of RWCV, RGRW, and RGILS methods does not decline with the increase of breast density. But the performance of CVAC and TMDP methods falls off on masses with denser tissues.

Besides quantitatively compared methods in Table 2, we qualitatively compare other two recent methods with our method. Zhang *et al.* (2010) proposed the method that can detect not only clear masses, but also masses hidden by gland tissues in a mammogram. But the segmentation results were not accurate enough. Moreover, the spiculation structures were ignored by mean shift segmentation. Xu *et al.* (2011) adopted the marker-controlled watershed method to avoid the over-segmentation problem of the traditional watershed. Since the watershed transformation was computed on the smoothed morphological gradient image of the original ROI, some subtle structures of masses might be ignored. In addition, it was observed that surrounding dense background tissues inside the external marker could result in the failure of segmentation. Due to the complexity of masses in mammograms, it is often difficult to obtain satisfactory segmentation results by using only one method (Song *et al.*, 2010). By using the complementary nature of the random walks and CV active model, our segmentation method is more adaptive to different masses.

4.3 Parameters and initialization perturbations

Fig. 10 shows the sensitivity of the RWCV method with respect to different model parameters μ, β (Table 3). As shown in Fig. 10a, the average performance of RWCV declines with the increase of μ from 0.05×255^2 to 0.2×255^2. In Fig. 10b, changing β by ±67% does not result in significant changes of the average AOM and AMED.

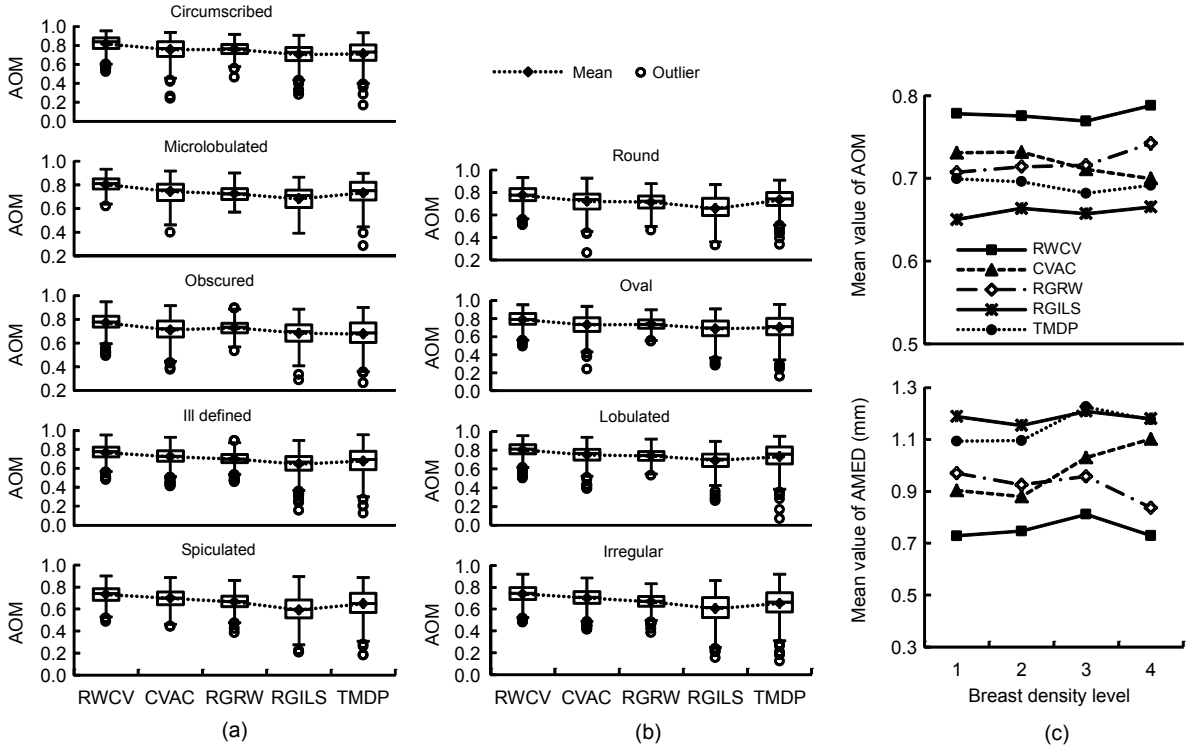

Fig. 9 Segmentation performance of different methods on five margin types of masses (a), four shape types of masses (b), and four breast density levels (c)

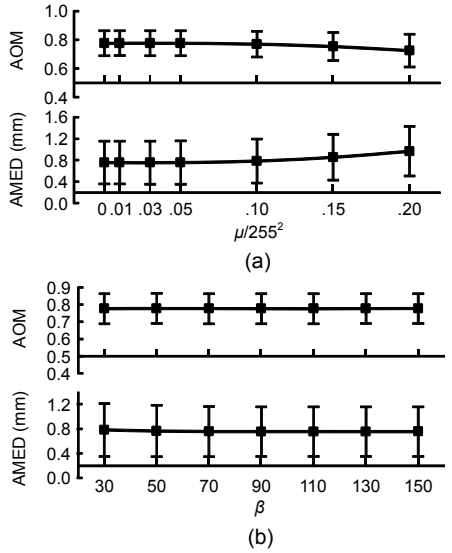

Fig. 10 Mean and standard deviation (SD) values of AOM and AMED for different μ (a) and β (b)

In a CAD system, the lesion center is provided by the previous lesion detection result. Therefore, there are perturbations in the placement of the mass center. In our experiments, the location of the mass center is shifted in a random direction with a random magnitude. We reject the perturbation which is outside the manual annotation of mass, since the detected region would not be considered as mass if the geometric center is outside the manual annotation in some detection methods (Oliver *et al.*, 2010). For each ROI, 20 segmentation results are recomputed according to 20 shifted center points. We randomly select 50 benign and 50 malignant ROIs to be a smaller test dataset. Fig. 11 shows the average performance with respect to the center perturbations over 100 tested ROIs. Overall, the performance declines with the increase of shift magnitude. The average change of AOM is less than 10% if $\Delta R/R_{\text{mass}}<70\%$.

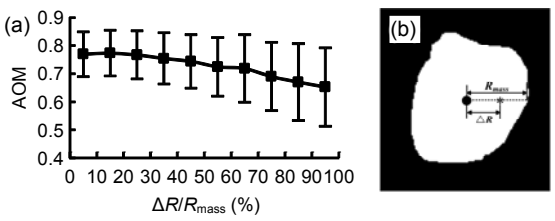

Fig. 11 The average performance with respect to the center perturbations over 100 tested ROIs

(a) Changes of AOM mean and SD as the mass center is perturbed; (b) Illustration of ΔR and R_{mass} (* represents the shifted center point, and ● represents the geometric center of manual outline)

Recalling from Section 3.1, the area of the initial ellipse is used to extract the seeds of the initial random walks from the isocontour map. Therefore, we first test the performance of the initial ellipse by the AOM metric. Then, the AOM values of all the initial ellipses are separated into five ranges: (0, 0.4], (0.4, 0.5], (0.5, 0.6], (0.6, 0.7], (0.7, 1). Fig. 12 shows the performance of segmentation results with initial ellipse in different AOM ranges. It can be seen that the segmentation results with an inaccurate initial ellipse show lower performance.

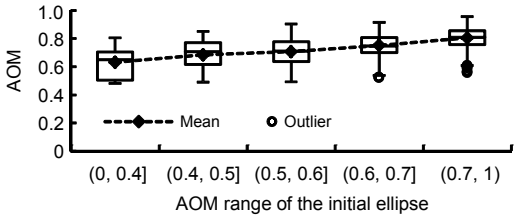

Fig. 12 Segmentation results in different AOM ranges of the initial ellipse

4.4 Computation time

The implementation of this study was performed on a computer with quad 2.67 GHz Intel® Xeon® processors. The operating system is Microsoft® Windows® XP. All five methods were programmed in MATLAB® R2010a. The average processing time and standard deviations of the five methods for one ROI are shown in Table 4. Due to the combination of two algorithms, our RWCV method shows the lowest computation efficiency.

Table 4 Average processing time and standard deviation of one ROI for five methods

Method	Average time±SD (s)
RWCV	5.143±1.102
CVAC	3.894±0.824
RGRW	2.246±0.438
RGILS	4.736±0.995
TMDP	0.967±0.154

5 Discussion and conclusions

In this study, we propose a hybrid segmentation method based on the random walks algorithm and CV active contour model (RWCV) for automatic mass segmentation. The seeds of the random walks

algorithm are first generated automatically from the isocontour map. Then, the energy function of the CV model is modified by the probability matrices produced by random walks. The modification can prevent the contour leaking problem. Moreover, some ambiguous characteristics in the periphery of the mass can be captured by updating the probability matrices during contour evolution. The proposed RWCV method is compared with basic random walks and CV model based methods (RGRW and CVAC), as well as other two existing methods (RGILS and TMDP). The experimental results indicate that the proposed RWCV method provides more accurate results than the other four methods.

In the RGRW method, the background seeds are defined as a shape constraint to prevent contour leaking. But some necessary image preprocessing steps blur the subtle structures and suppress the ambiguous margins of the masses. Even without preprocessing, it is difficult to label the seeds for these subtle or ambiguous structures by region growing. Therefore, the segmentation results of the RGRW method are prone to shrink to the core regions of masses, and ignore some dimmer or subtle information in the periphery (Figs. 7 and 8).

Based on the contour evolution technique, the CV active contour model is more capable to deal with complex shapes or subtle structures of masses. But it still cannot work well because of the contour leaking problem. As we can see in Fig. 9c, the performance of the CVAC method obviously falls off with the increase of breast tissue density, since denser tissues possess similar appearances to mass in mammograms, which can result in a contour leaking problem.

In the RGILS method, the radial gradient index (RGI) algorithm is applied to yield an initial contour for level set segmentation. The RGI algorithm works well for lesions with circular-like shapes and smooth margins. But the initial contours are usually undergrown for lesions with irregular shapes and spiculated margins (Yuan *et al.*, 2007). Moreover, the background correction based on initial contours may suppress the margin region of mass. Therefore, the segmented contours of the RGILS method also approach more to the inner region of mass, and result in worse performance on M_{FN} evaluation (Figs. 7 and 8).

The definition of the local cost function is critical for the dynamic programming based method. In the TMDP method, the template matching algorithm is first used to produce a rough region of mass in the ROI, which can constrain the range of boundary searching and provide a method to estimate the local cost of candidate pixels (Song *et al.*, 2010). But the adaptability and robustness of the local cost function are not very good. According to our experiments, some irrelevant pixels with strong gradient magnitude can interfere with the results of the TMDP method. Moreover, it is also difficult for this method to capture the boundaries of masses with complex shapes.

The margin and shape characteristics are primary criteria for the distinction of benign and malignant masses. As shown in Figs. 9a and 9b, our method shows better performance on different margin and shape types of masses. Therefore, the features extracted based on the segmentation results of our method should be more feasible for lesion classification. All five methods show poorer performance on masses with spiculated margins. Unlike the main parts of masses, spiculations present in mammograms as nearly linear filaments extending from the mass periphery, and they are often ill defined with poor contrast (Ball and Bruce, 2007b). In our RWCV method, probability matrices updates during contour evolution let the modified CV model explore the periphery of mass, so that some subtle and ambiguous structures can be captured. The segmentation performance of our RWCV method on spiculated masses is a bit better than those of the other four methods, but still not good enough. Clearly, some other methods should be developed to capture the spiculations, since the appearances of spiculations are different from the main parts of masses in mammograms. This aspect will be studied in our future work.

The CV model and random walks algorithm require several parameters be determined. In the CV model, parameter μ controls the smoothness of the final contour. A larger μ will result in a smoother contour. As some important features of masses, such as spiculation, characterize the fine details of the lesion margins, the value of μ should not be too large. In our study, we keep both λ_1 and λ_2 in Eq. (10) to one ($\lambda_1=\lambda_2=1$) since we equally consider the contributions of the inside and outside regions of the contour. The value β in Eq. (2) is the only free parameter of the random walks algorithm. The performance of the RWCV method is stable with respect to the change of

β (Fig. 10).

The center of the lesion and the initial ellipse can be considered as the initialization of the following hybrid segmentation process in the proposed RWCV method. As shown in Fig. 11, greater deviation from the actual mass center produces greater decline of the average segmentation performance. According to our experiments, the center perturbations inside the highlight core regions of masses show less influence on the segmentation performance. Therefore, it will be better if intensity information is also taken into account to determine the center of lesion in the CAD system. Moreover, some enhancement algorithms can be employed to improve the contrast of mass. As described in Section 3.2, the seeds of the initial random walks are extracted from the isocontour map according to the area of the initial ellipse A_{ellipse}. Therefore, if A_{ellipse} is smaller than the actual area of mass, the initial contour would like to approach more to the inner region of mass. According to our experiments, this undersegmentation problem can be compensated to a certain degree in the following contour evolution process of the modified CV model. But if A_{ellipse} is much larger than the mass area, so that the mass seeds of the initial random walk are outside the mass region, there will be an oversegmentation problem for the final result.

As a combination of two algorithms, the proposed RWCV method needs more computation time than other methods. Therefore, some potential approaches are considered to optimize the method. First, all the algorithms are programmed in MATLAB codes. Therefore, some more efficient coding schemes can be considered by using advanced programming languages (e.g., C/C++). Second, both the mass and background seeds are defined as closed contours in this study. Since each segmented region generated by random walks is guaranteed to be connected to seeds with the same label (Grady, 2006), the pixels outside the background seeds can be labeled directly as background. In a similar way, the pixels inside the mass seeds can also be labeled directly as mass. These pixels do not need to be involved in the computation of random walks. In addition, the random walks algorithm can be sped up by the graphics processing unit (GPU) for massive data processing (Grady, 2006).

Certainly, there are still some limitations in this approach. The performance on masses with spiculated margins or irregular shapes still needs to be improved. Some other preprocessing methods should also be considered to improve the stability of our method. Another limitation of our method is related to other stages in the CAD system. In practical CAD systems, the ROI may be obtained according to the previous detection stage. In addition, the segmented contours produced by the segmentation method are used in the latter lesion classification stage. In this sense, experiments in our study do not quantify the performance of our method for the detection or classification of breast mass. However, detection and classification of breast mass are complex tasks. The performance of different detection algorithms strongly influences the performance of segmentation, and the classification of breast mass depends not only on the segmentation result but also on the particular features and classifiers employed. Hence, our segmentation method is evaluated independently of the detection or classification stages of the CAD system, and the methods being compared all focus on the segmentation of mass in manually defined ROI. These limitations will be explored in our future work.

References

American Cancer Society, 2011. Cancer Facts & Figures 2011. Available from http://www.cancer.org/acs/groups/content/@epidemiologysurveilance/documents/document/acspc-029771.pdf

Ball, J.E., Bruce, L.M., 2007a. Digital Mammographic Computer Aided Diagnosis (CAD) Using Adaptive Level Set Segmentation. 29th Annual Int. Conf. of the IEEE Engineering in Medicine and Biology Society, p.4973-4978. [doi:10.1109/IEMBS.2007.4353457]

Ball, J.E., Bruce, L.M., 2007b. Digital Mammogram Spiculated Mass Detection and Spicule Segmentation Using Level Sets. 29th Annual Int. Conf. of the IEEE Engineering in Medicine and Biology Society, p.4979-4984. [doi:10.1109/IEMBS.2007.4353458]

Cao, Y., Hao, X., Xia, S., 2009. An improved region-growing algorithm for mammographic mass segmentation. *SPIE*, **7497**:74971O-1-74971O-7.

Cao, Y., Hao, X., Zhu, X., Xia, S., 2011. Mammographic mass segmentation algorithm based on automatic random walks. *J. Zhejiang Univ. (Eng. Sci.)*, **45**(10):1753-1760 (in Chinese). [doi:10.3785/j.issn.1008-973X.2011.10.009]

Chan, T.F., Vese, L.A., 2001. Active contours without edges. *IEEE Trans. Image Process.*, **10**(2):266-277. [doi:10.1109/83.902291]

Chaudhury, K.N., Ramakrishnan, K.R., 2007. Stability and convergence of the level set method in computer vision. *Pattern Recogn. Lett.*, **28**(7):884-893. [doi:10.1016/j.patrec.2006.12.003]

Domínguez, A.R., Nandi, A.K., 2007. Improved dynamic-programming-based algorithms for segmentation of masses in mammograms. *Med. Phys.*, **34**(11):4256-4269. [doi:10.1118/1.2791034]

Grady, L., 2006. Random walks for image segmentation. *IEEE Trans. Pattern Anal. Mach. Intell.*, **28**(11):1768-1783. [doi:10.1109/TPAMI.2006.233]

Guliato, D., Rangayyan, R.M., Carnielli, W.A., Zuffo, J.A., Desautels, J.E.L., 1998. Segmentation of Breast Tumors in Mammograms by Fuzzy Region Growing. Proc. 20th Annual Int. Conf. of the IEEE Engineering in Medicine and Biology Society, p.1002-1005. [doi:10.1109/IEMBS.1998.745618]

Guliato, D., Rangayyan, R.M., Carnielli, W.A., Zuffo, J.A., Desautels, J.E.L., 2003. Segmentation of breast tumors in mammograms using fuzzy sets. *J. Electron. Imag.*, **12**(3):369-378. [doi:10.1117/1.1579017]

Hao, X., Xia, S., 2009. A dynamic programming algorithm for mass segmentation on mammograms based on contour supervision. *Sci. Technol. Rev.*, **27**(21):56-60 (in Chinese).

Heath, M., Bowyer, K., Kopans, D., Kegelmeyer, W.P., Moore, R., Chang, K., MunishKumaran, S., 1998. Current Status of the Digital Database for Screening Mammography. Proc. 4th Int. Workshop on Digital Mammography, p.457-460.

Heath, M., Bowyer, K., Kopans, D., Moore, R., Kegelmeyer, W.P., 2000. The Digital Database for Screening Mammography. Proc. 5th Int. Workshop on Digital Mammography, p.212-218.

Hong, B.W., Sohn, B.S., 2010. Segmentation of regions of interest in mammograms in a topographic approach. *IEEE Trans. Inf. Technol. Biomed.*, **14**(1):129-139. [doi:10.1109/TITB.2009.2033269]

Kupinski, M.A., Giger, M.L., 1998. Automated seeded lesion segmentation on digital mammograms. *IEEE Trans. Med. Imag.*, **17**(4):510-517. [doi:10.1109/42.730396]

Oliver, A., Freixenet, J., Martí, J., Pérez, E., Pont, J., Denton, E.R.E., Zwiggelaar, R., 2010. A review of automatic mass detection and segmentation in mammographic images. *Med. Image Anal.*, **14**(2):87-110. [doi:10.1016/j.media.2009.12.005]

Osher, S., Sethian, J.A., 1988. Fronts propagating with curvature-dependent speed: algorithms based on Hamilton-Jacobi formulations. *J. Comput. Phys.*, **79**(1):12-49. [doi:10.1016/0021-9991(88)90002-2]

Petrick, N., Chan, H.P., Sahiner, B., Helvie, M.A., 1999. Combined adaptive enhancement and region-growing segmentation of breast masses on digitized mammograms. *Med. Phys.*, **26**(8):1642-1654. [doi:10.1118/1.598658]

Qian, W., Li, L., Clark, L.P., 1999. Image feature extraction for mass detection in digital mammography: influence of wavelet analysis. *Med. Phys.*, **26**(3):402-408. [doi:10.1118/1.598531]

Sahiner, B., Petrick, N., Chan, H.P., Hadjiiski, L.M., Paramagul, C., Helvie, M.A., Gurcan, M.N., 2001. Computer-aided characterization of mammographic masses: accuracy of mass segmentation and its effects on characterization. *IEEE Trans. Med. Imag.*, **20**(12):1275-1284. [doi:10.1109/42.974922]

Song, E., Jiang, L., Jin, R., Zhang, L., Yuan, Y., Li, Q., 2009. Breast mass segmentation in mammography using plane fitting and dynamic programming. *Acad. Radiol.*, **16**(7):826-835. [doi:10.1016/j.acra.2008.11.014]

Song, E., Xu, S., Xu, X., Zeng, J., Lan, Y., Zhang, S., Hung, C.C., 2010. Hybrid segmentation of mass in mammograms using template matching and dynamic programming. *Acad. Radiol.*, **17**(11):1414-1424. [doi:10.1016/j.acra.2010.07.008]

te Brake, G.M., Karssemeijer, N., 2001. Segmentation of suspicious densities in digital mammograms. *Med. Phys.*, **28**(2):259-266. [doi:10.1118/1.1339884]

Timp, S., Karssemeijer, N., 2004. A new 2D segmentation method based on dynamic programming applied to computer aided detection in mammography. *Med. Phys.*, **31**(5):958-971. [doi:10.1118/1.1688039]

Wang, Y., Tao, D., Gao, X., Li, X., Wang, B., 2011. Mammographic mass segmentation: embedding multiple features in vector-valued level set in ambiguous regions. *Pattern Recogn.*, **44**(9):1903-1915. [doi:10.1016/j.patcog.2010.08.002]

Xiao, M., Xia, S., Wang, S., 2005. Geometric Active Contour Model with Color and Intensity Priors for Medical Image Segmentation. 27th Annual Int. Conf. of the Engineering in Medicine and Biology Society, p.6496-6499. [doi:10.1109/IEMBS.2005.1615987]

Xu, S., Liu, H., Song, E., 2011. Marker-controlled watershed for lesion segmentation in mammograms. *J. Dig. Imag.*, **24**(5):754-763. [doi:10.1007/s10278-011-9365-2]

Xu, W., Xia, S., Duan, H., Xiao, M., 2006. Segmentation of mass in mammograms using a novel intelligent algorithm. *Int. J. Pattern Recogn. Artif. Intell.*, **20**(2):255-270. [doi:10.1142/S0218001406004648]

Yuan, Y., Giger, M.L., Li, H., Suzuki, K., Sennett, C., 2007. A dual-stage method for lesion segmentation on digital mammograms. *Med. Phys.*, **34**(11):4180-4193. [doi:10.1118/1.2790837]

Zhang, Y., Tomuro, N., Furst, J., Stan Raicu, D., 2010. Image enhancement and edge-based mass segmentation in mammogram. *SPIE*, **7623**:76234P-1-76234P-8.